Modelling the irreversible response of magnetically ordered materials: a Preisach-based approach

2001 J. Phys.: Condens. Matter 13 3443

(http://iopscience.iop.org/0953-8984/13/14/317)

INSTITUTE OF PHYSICS PUBLISHING JOURNAL OF PHYSICS: CONDENSED MATTER

J. Phys.: Condens. Matter **13** (2001) 3443–3460 www.iop.org/Journals/cm PII: S0953-8984(01)20076-9

Modelling the irreversible response of magnetically ordered materials: a Preisach-based approach

T Song[1], **R M Roshko**[1] **and E Dan Dahlberg**[2]

[1] Department of Physics and Astronomy, University of Manitoba, Winnipeg, MB, R3T 2N2, Canada
[2] School of Physics and Astronomy, University of Minnesota, Minneapolis, MN 55455, USA

Received 14 December 2000, in final form 12 February 2001

Abstract

We present a general theoretical framework, based on the Preisach model of hysteresis, for describing irreversible phenomena in magnetically ordered materials, which includes the effects of the critical ordering temperature T_C. The model is based on the premise that the free energy landscape can be decomposed into an ensemble of bistable Barkhausen elements, each characterized by two energy barriers which are defined by local anisotropy and interaction fields. The free energy landscape has an explicit temperature dependence which originates from the critical growth of the spontaneous moment below the critical temperature T_C, and thermal overbarrier fluctuations are responsible for relaxing the system towards equilibrium. The theory identifies certain fundamental characteristic energies which play a primary role in determining the principal features of the magnetic response. The model is able to replicate a broad spectrum of behaviour observed experimentally in the field and temperature dependence of magnetic response functions such as the field cooled and zero-field cooled moment and the major hysteresis loop, in a wide variety of magnetic materials, including very specific experimental anomalies and trends, and provides a rigorous theoretical framework which quantifies the interpretation of the experimental data.

1. Introduction

The vast majority of magnetic materials which form the subject of current investigation, whether for fundamental or technological reasons, are *magnetically ordered*, in the sense that they possess a characteristic critical temperature T_C at which the permanent atomic moments undergo a sudden, spontaneous, cooperative alignment, driven by the exchange interaction. Below T_C, the material consists of uniformly magnetized regions, which may be either discrete particles or magnetic domains, or some mixture of these. In general, the state of a magnetic system in a given external field h_a at a given temperature T cannot be completely specified by global response functions such as the total system moment m, since each value of m can be realized by a multiplicity of distinct configurations of uniformly magnetized regions. Each of

0953-8984/01/143443+18$30.00

these configurations is *metastable* in the sense that it corresponds to a local minimum in the free energy landscape in a multidimensional configuration space. These metastable minima are separated by energy barriers, due to anisotropy and domain wall pinning effects, which trap the system temporarily in a particular configuration and prevent it from exploring all of its configuration space ergodically, and thus from reaching thermal equilibrium within the timescale t_{exp} of a given experiment. Each energy barrier W is characterized by a *blocking temperature* $T_B < T_C$, below which thermal fluctuations are insufficient to excite an overbarrier transition. Furthermore, the free energy landscape itself depends explicitly on temperature, and all of the free energy barriers must collapse along with the spontaneous moment of the domains or particles as the critical temperature is approached from below. Thus, in response to changes in field or temperature, the system evolves from one configuration to another along a very complex path in a multivalleyed configuration space, driven in part by field-induced distortions of the free energy landscape which extinguish local transition barriers, and in part by thermal overbarrier activation events. This path is highly sensitive to the precise sequence of application of the external stimuli, as well as to the timescale t_{exp} of the experiment, and this situation is reflected in the multivaluedness of experimental response functions such as $m(h_a, T)$, a phenomenon known as *hysteresis*.

The Preisach model of hysteresis [1, 2] provides the physical and mathematical foundations for constructing a comprehensive theoretical description of irreversibility in magnetically ordered materials, which incorporates all of the essential physical elements outlined above. The model assumes that the free energy landscape, no matter how complex, can be decomposed into an ensemble of elementary bistable fragments [2–4], each characterized by two stable states and by two free energy barriers W_+ and W_-, which inhibit transitions between the states. A given magnetic material is characterized by a particular *distribution* $f(W_+, W_-)$ of these energy barriers. Transitions between the two levels of a subsystem must be activated by some combination of *field energy* and *thermal energy*, and the model provides a uniquely graphical representation of these activation conditions, and a powerful mathematical algorithm for computing the response of the entire ensemble under a variety of common experimental protocols. When the spontaneous moment of the subsystems and the distribution of subsystem free energy barriers are allowed to evolve explicitly with temperature, the model is able to replicate in detail many of the structural features which characterize the irreversible response of a broad spectrum of magnetically ordered systems, and identifies certain fundamental characteristic energies which play a particularly crucial role in shaping the response.

2. The model

The Preisach model [1, 2] decomposes all magnetic systems into an ensemble of bistable subsystems, each characterized by a moment μ, two states $\varphi = \pm\mu$ and a double well free energy profile with two zero-field transition barriers W_+ and W_-, as shown in figure 1. The barriers can be represented either by their *equivalent fields* $\alpha = W_-/\mu$ and $\beta = -W_+/\mu$, or by a *coercive field* $H_c = (W_+ + W_-)/2\mu$ and an *asymmetry field* $h_i = (W_+ - W_-)/2\mu$. In essence, the model reduces the magnetizing process to a sequence of elementary Barkhausen instabilities of magnitude μ. The coercive field h_c functions like an *intrinsic anisotropy field*, which stabilizes the two moment orientations $\varphi = \pm\mu$, and measured the *energy dissipated* as heat in a Barkhausen transition [2], while the asymmetry field h_i behaves like a *local interaction field* due to neighbouring subsystems, which lifts the degeneracy of the two valleys, and measures the *energy stored* in a transition [2]. A given magnetic material is identified by a particular *distribution* $f(W_+, W_-)$ of free energy barriers, or equivalently by a distribution of the characteristic fields, either $p(\alpha, \beta)$ or $p(h_c, h_i)$.

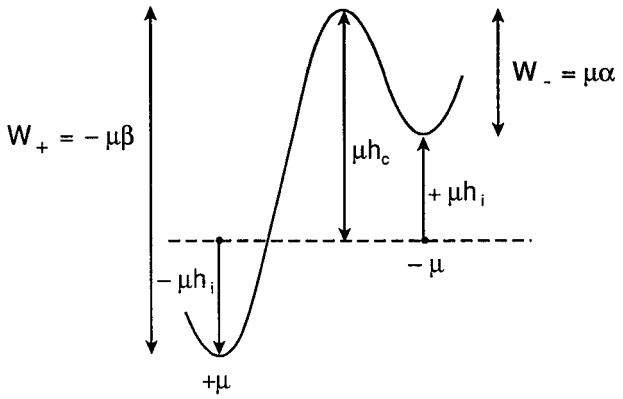

Figure 1. The free energy profile in zero applied field for an elementary Barkhausen subsystem, with two states $\varphi = \pm\mu$ separated by energy barriers $W_- = \mu\alpha = \mu(h_c - h_i)$ and $W_+ = -\mu\beta = \mu(h_c + h_i)$.

Transitions between the two states of a subsystem require excitation over the barriers $W_\pm$ by some combination of *field energy* and *thermal energy*. In particular, the application of an external field h_a shifts the energy of the $\varphi = +\mu$ state by $-\mu h_a$, and the energy of the $\varphi = -\mu$ state by $+\mu h_a$, and thus modifies all the subsystem energy barriers from $W_\pm$ to $W'_+ = -\mu(\beta - h_a)$ and $W'_- = \mu(\alpha - h_a)$. For subsystems with $\beta > h_a$, $W'_+ < 0$, and only the $\varphi = -\mu$ state is accessible. Similarly, for subsystems with $\alpha < h_a$, $W'_- < 0$ and only the $\varphi = +\mu$ state is accessible. All subsystems with $(h_a < \alpha < \infty, -\infty < \beta < h_a)$ are *bistable* in the sense that they have *two* accessible states and *two* positive energy barriers $W'_\pm > 0$. For the *bistable* subsystems, transitions may also be induced *thermally* if the system is at a finite temperature T. For an experiment with a characteristic time constant t_{exp}, thermal transitions are limited to those barriers which are less than or equal to the *effective thermal fluctuation energy* $W^*(T) = k_B T \ln(t_{exp}/\tau_0)$ [3, 4]. These thermal transitions may also be described by an *equivalent thermal viscosity field* $h^*_T = W^*/\mu$, which defines the maximum *field barrier* which can be activated at temperature T. Since each bistable subsystem has two energy barriers, a larger barrier $W_L = \mu(h_c + |h_i + h_a|)$ and a smaller barrier $W_S = \mu(h_c - |h_i + h_a|)$, there are two thermal excitation conditions, $W^* = W_L$, which yields $h^*_{TL} = h_c + |h_i + h_a|$, and $W^* = W_S$, which yields $h^*_{TS} = h_c - |h_i + h_a|$.

Both the field and thermal excitation conditions can be represented graphically in the Preisach plane [1, 2], in which each subsystem is located with respect to orthogonal coordinate axes by either its characteristic fields (h_c, h_i) or by the equivalent fields (α, β) which reduce the barriers $W'_\pm$ to zero. Figure 2 shows the Preisach plane in a positive field $h_a > 0$ at a finite temperature T. The quadrant enclosed between the boundaries $\alpha = h_a$ and $\beta = h_a$ contains the *bistable* subsystems, which can potentially occupy either state $\varphi = \pm\mu$. For a given temperature T, there are two thermal excitation boundaries, the dashed boundaries h^*_{TS}, which identify those subsystems whose *lower* energy barrier matches $W^*(T)$, and the solid boundaries h^*_{TL}, which are the locus of subsystems whose *higher* barrier matches $W^*(T)$. Subsystems which lie to the left or above the h^*_{TS} boundaries have a thermally active lower barrier and a thermally inactive higher barrier, and consequently occupy their *lower* energy state exclusively, while those subsystems within the shaded region have *two* thermally active barriers, *equilibrium* Boltzmann level populations and a *superparamagnetic* response function $\varphi_{sp} = \mu(T)\tanh[\mu(T)(h_a + h_i)/k_B T]$.

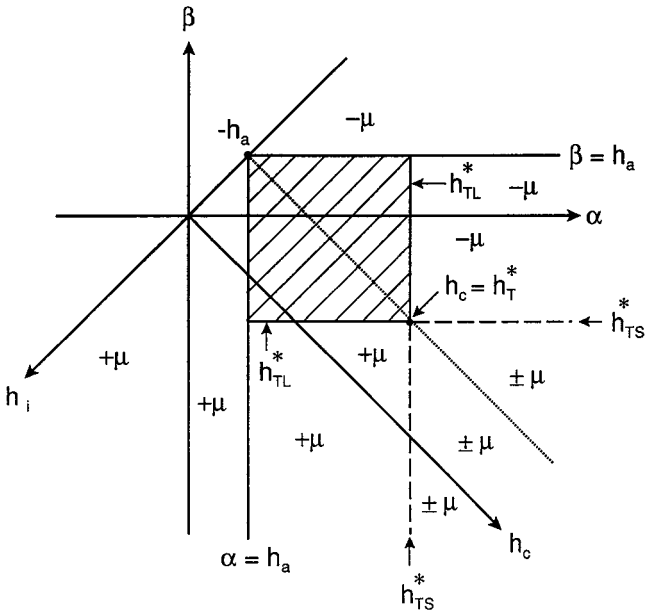

Figure 2. The Preisach plane in a positive applied field h_a. The quadrant defined by $(h_a < \alpha < \infty, -\infty < \beta < h_a)$ consists of bistable subsystems with two positive energy barriers. The two sets of thermal boundaries labelled h^*_{TL} and h^*_{TS} are the loci of subsystems whose larger and smaller energy barriers, respectively, match the thermal fluctuation energy $W^*(T) = \mu h^*_T$ at temperature T. The shaded area identifies those subsystems which are in thermal equilibrium at temperature T.

The Preisach diagram in figure 2 provides the basis for a description of common experimental protocols, such as field cooling (FC), zero-field cooling (ZFC) and moment–field isotherms. The system response upon warming in a field $h_a > 0$, after first cooling to $T = 0$ in zero field, is replicated by simply translating the vertex $h_c = h^*_T$ in figure 2 *outward* along the dotted diagonal $h_i = -h_a$ in the direction of increasing h_c, starting from $h_c = h^*_T = 0$. The subsystems behind the thermal instability boundaries are activated into their appropriate states as shown, while those in the region of double occupancy ($\varphi = \pm\mu$) in front of the dashed boundaries retain their zero-field cooled configuration. To simulate field cooling (FC) from a high temperature, the vertex $h_c = h^*_T$ is translated *inward* starting from $h_c = h^*_T = \infty$, where the entire bistable quadrant is superparamagnetic. This procedure eliminates the possibility of double occupancy ($\varphi = \pm\mu$) in front of the dashed thermal boundaries and, with the exception of the superparamagnetic region, forces all subsystems below the diagonal $h_i = -h_a$ into their $\varphi = +\mu$ state, and all subsystems above the diagonal into their $\varphi = -\mu$ state. To generate the magnetic response at a fixed temperature T to any sequence of field applications and reversals, including the initial magnetizing curve, major and minor hysteresis loops and remanences, the vertex $h_i = -h_a$ is shifted in the appropriate direction along the h_i-axis, keeping h^*_T fixed. This process has a *directional dependence*, in the sense that under ZFC conditions the configuration of the Preisach plane in a given field h_a in the region of double occupancy ($\varphi = \pm\mu$) is not unique, but rather depends upon whether the field was approached from above or below. For all of these protocols, the system response is obtained by weighting the state $\varphi(h_c, h_i, h_a, T)$ of each

subsystem by the Preisach distribution $p(h_c, h_i)$ and integrating over the entire Preisach plane:

$$m = \int_0^{\infty} \mathrm{d}h_c \int_{-\infty}^{+\infty} \mathrm{d}h_i \; \varphi(h_c, h_i, h_a, T)\, p(h_c, h_i). \tag{1}$$

Thermal effects are not limited to overbarrier fluctuations alone. In fact, both the spontaneous moment μ of the subsystems, and the subsystem free energy barriers $W_{\pm}$, are expected to depend explicitly on temperature. The variation of the spontaneous moment is related to the existence of the critical temperature, and is assumed to obey a power law of the form $\mu(T) = \mu_0(1 - T/T_c)^{\Gamma}$, where $\Gamma \sim 1/3$ for magnetic systems. If we assume, in keeping with standard practice [2], that the Preisach distribution is a product of Gaussian coercive and interaction field distributions:

$$p(h_c, h_i) = (2\pi\sigma_c^2)^{-1/2} \exp\left[-\frac{(h_c - \bar{h}_c)^2}{2\sigma_c^2} \right] (2\pi\sigma_i^2)^{-1/2} \exp\left[-\frac{(h_i - km)^2}{2\sigma_i^2} \right] \tag{2}$$

which includes long range mean-field-like interactions $\bar{h}_i = km$ proportional to the total induced system moment m [5], then the temperature dependence of the free energy barriers $W_{\pm}(T)$ is described by introducing similar power law temperature dependences into the Preisach distribution parameters:

$$\left\{ \begin{array}{l} \bar{h}_c = \bar{h}_{c0} \left(1 - \dfrac{T}{T_C} \right)^{\Gamma_c} \\ \sigma_c = \sigma_{c0} \left(1 - \dfrac{T}{T_C} \right)^{\Gamma_c'} \\ \sigma_i = \sigma_{i0} \left(1 - \dfrac{T}{T_C} \right)^{\Gamma_i} \end{array} \right\}. \tag{3}$$

Thus both distributions collapse into δ-functions as $T \to T_C$ from below, as expected on physical grounds. This is illustrated schematically in figure 3. The thermal viscosity field h_T^*, which describes the effects of thermal fluctuations, is related to the thermal fluctuation energy $W^*(T)$ through $h_T^* = W^*(T)/\mu_0 = (k_B T/\mu_0) \ln(t_{exp}/\tau_0)$. Similarly, the temperature dependence of the free energy barriers $W_{\pm}(T)$ is defined by the temperature dependence of the characteristic fields $h_c(T)$ and $h_i(T)$ through the relation $W_{\pm}(T) = \mu_0[h_c(T) \pm h_i(T)]$.

3. Numerical simulations

According to the model, the temperature dependence of the magnetic response below the critical temperature T_C has two sources: (a) the variation with temperature of properties which are *intrinsic* to the system, such as the spontaneous moment $\mu(T)$ and the free energy barriers $W_{\pm}(T)$, and (b) thermal fluctuations, which effectively reduce all of the subsystem energy barriers by $W^*(T)$ and which are *extrinsic* to the system. The model contains two fundamental *characteristic energies*, which form a natural basis for a quantitative comparison of the two thermal processes and their effects on the magnetic response functions. One of these characteristic energies is the *critical thermal fluctuation energy* $W_C \equiv k_B T_C \ln(t_{exp}/\tau_0)$, which measures the *highest* energy barrier which can be thermally activated for a system with a critical temperature T_C. The other is the *mean zero-temperature anisotropy barrier* $\overline{W}_a(0) \equiv \mu_0 \bar{h}_{c0}$, which places an *upper limit* on the height to which the barriers of a given system can grow, and thus measures, in some sense, the ability of a system to resist the equilibrating effects of thermal fluctuations. The relative strength of the two characteristic energies is measured by the dimensionless parameter $\eta \equiv \overline{W}_a(0)/W_C$.

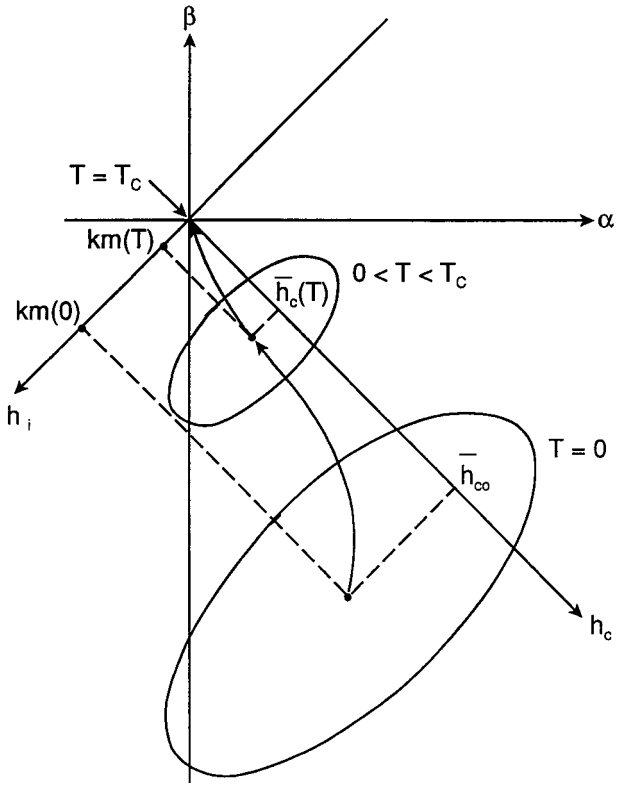

Figure 3. A schematic representation of the collapse of the Preisach distribution $p(h_c, h_i)$ as the temperature T approaches the critical temperature T_C from below. Both the mean coercive field $\bar{h}_c(T)$ and the mean interaction field $\bar{h}_i(T) = km(T)$ vanish as $T \to T_C$, as do the dispersions $\sigma_c(T)$ and $\sigma_i(T)$.

In order to appreciate the physical significance of these two characteristic energies, it is necessary to compare the temperature dependence of the two competing thermal processes. Figure 4 shows the temperature dependence, on a dimensionless temperature scale T/T_C, of a *band of anisotropy barriers* which lie between the two boundary curves $W_a^{\pm}(T) = [\overline{W}_a(0) \pm 0.4\overline{W}_a(0)](1 - T/T_C)^{1/3}$. The figure also shows the effective thermal fluctuation energy $W^*(T) = k_B T \ln(t_{exp}/\tau_0) = [\overline{W}_a(0)/\eta](T/T_C)$ for two extreme situations, $\eta = 0.2$ and $\eta = 4.0$, plotted as a function of T/T_C, and represented by the two straight lines in figure 4. If we temporarily neglect the effects of interaction fields h_i and the applied field h_a, neither of which are *fundamental* to the present discussion, then the intersection of $W^*(T)$ with the two boundary curves $W_a^{\pm}(T)$ defines the range of *excitation* or *blocking temperatures* T_B for the system, which lie roughly between the two limits T_{BL} and T_{BH}.

For the system with $\eta = 0.2$, the critical growth of the spontaneous moment and of the free energy landscape occurs almost entirely *above* the highest blocking temperature T_{BH}, where $W^*(T) > W_a^+(T)$ and hence where thermal energy is sufficient to activate *all* of the free energy barriers, so this system will be in thermal equilibrium and will exhibit a *reversible superparamagnetic* response throughout the landscape development phase. Below T_{BH}, where the system exhibits hysteresis, the free energy barriers evolve very slowly with temperature in comparison with the thermal fluctuation energy $W^*(T)$, as shown in figure 4. Consequently,

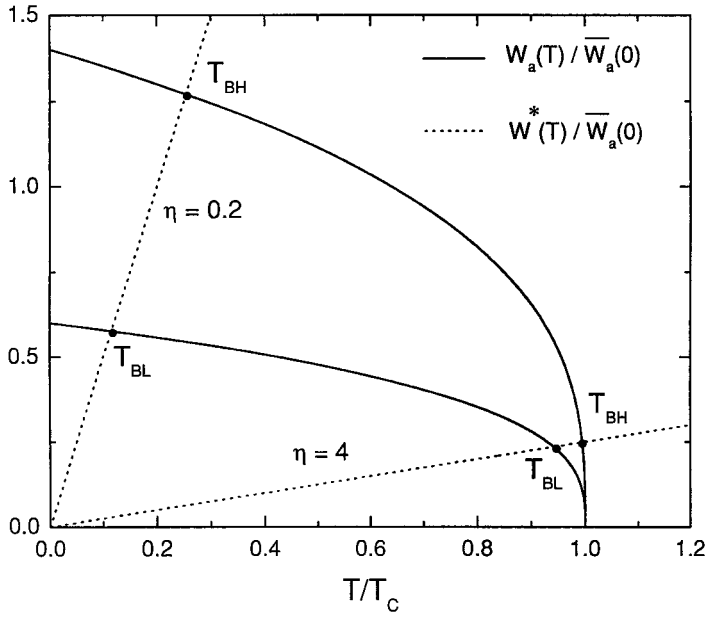

Figure 4. The temperature dependence of a band of anisotropy barriers between $W_a^{\pm}(T) = \overline{W}_a(0)(1 \pm 0.4)(1 - T/T_C)^{1/3}$ (solid curves), and the temperature dependence of the effective thermal fluctuation energy $W^*(T) = k_B T \ln(t_{exp}/\tau_0) = [\overline{W}_a(0)/\eta](T/T_C)$, for two limiting situations where $\eta = \overline{W}_a(0)/W_C = 0.2$ and $\eta = 4.0$.

the temperature dependence of the magnetic response functions (FC moment, ZFC moment, hysteresis loop and so on) originates almost exclusively from the thermal-fluctuation-assisted reduction in the *effective* barrier heights $W_{eff}(T) = W_a(T) - W^*(T)$, rather than from changes in the intrinsic properties of the subsystems with temperature. We refer to systems like this as *fluctuation-dominated* systems. As figure 4 suggests, when the system is cooled through T_C in zero applied field $h_a = 0$, blocking will proceed 'sequentially', with the highest barriers blocking first at T_{BH} and the smallest barriers blocking last at T_{BL}. Once the highest-barrier subsystems freeze, they are capable of generating *static* local interaction fields, which will lift the degeneracy of the energy levels of neighbouring smaller-barrier subsystems, causing them to freeze with *unequal* Boltzmann populations. Thus the structure of the ground state for this system may be characterized by highly *asymmetric* level populations close to $(1, 0)$ or $(0, 1)$, and this is the configuration which we have adopted for the purpose of these simulations.

By contrast, for the system with $\eta = 4.0$, the thermal fluctuation energy $W^*(T)$ intersects the barrier distribution $W_a^{\pm}(T)$ very close to T_C, during the *early stages* of the development process. For the case considered here, the temperature T at which the average energy barrier reaches the critical height W_C is given by $\overline{W}_a(T) = \mu_0 \bar{h}_c(T) = \overline{W}_a(0)(1 - T/T_C)^{1/3} = W_C = \frac{1}{4}\overline{W}_a(0)$, which yields $1 - T/T_C = (\frac{1}{4})^3 \cong 0.016$, that is, very close to T_C. As before, blocking occurs over a range of temperatures between T_{BL} and T_{BH}. However, in this case, the superparamagnetic regime ($T_{BH} \leqslant T \leqslant T_C$) is very narrow, and blocking is complete not far below T_C, so the temperature dependence of the magnetic response throughout the hysteretic regime ($T < T_{BH}$) is expected to be dominated by the evolution of the free energy barriers $W_a(T)$, that is, by changes in the *intrinsic* properties of the subsystems themselves with temperature, with only a minor contribution from thermal fluctuations $W^*(T)$, as a comparison of the changes in $W_a(T)$ and $W^*(T)$ with temperature in figure 4 clearly shows. We refer to

systems like this as *anisotropy-dominated* systems. Although blocking is expected to proceed 'sequentially' as before, the structure of the ground state in this type of system is much more difficult to predict, since rapid changes in the size of the spontaneous moment $\mu(T)$ throughout the blocking regime can potentially lead to considerable variation in the strength of the interaction fields produced by the blocked subsystems, and hence in the ability of a blocked subsystem to split the levels of neighbouring unblocked subsystems. Thus, the ground state level populations may vary from nearly *random* $(\frac{1}{2}, \frac{1}{2})$ if the interaction fields are weak, to highly asymmetric $(1, 0)$ or $(0, 1)$ if the interaction fields are strong. For reasons of computational simplicity, we adopt the latter configuration throughout.

While the model clearly admits a broad spectrum of behaviour, depending upon the specific values of the barrier distribution parameters and on the slope of the thermal fluctuation line $W^*(T)$ in figure 4, we will continue to focus our attention on the two limiting situations described above, since these are of particular interest from an experimental perspective. All systems are assumed to share a certain basic set of parameters $\bar{h}_{c0} = 1.0, \sigma_{c0} = 0.4, \sigma_{i0} = 0.02$ (all normalized to the real zero-temperature coercive field), $k_B T_C = 0.01$ (normalized to the real critical thermal energy), exponents $\Gamma = \Gamma_c = \Gamma'_c = \Gamma_i = \frac{1}{3}$ and an experimental time parameter $\Omega \equiv \ln(t_{exp}/\tau_0) = 25$ typical of static measurements. Variations in the ratio $\eta = \overline{W}_a(0)/W_C$ are accomplished by manipulating the spontaneous subsystem moment μ_0, so the ratios $\eta = 0.2$ and $\eta = 4.0$ correspond to $\mu_0 = 0.05$ and $\mu = 1.0$, respectively. Other parameters from the basic set are then varied as necessary in order to illustrate specific systematic effects. In discussing the behaviour of the FC and ZFC response, we will tend to focus on the low-field limit $h_a \ll \bar{h}_{c0}$, where thermally induced effects dominate over field-induced effects.

Figure 5 shows a comparison of the temperature dependence of the FC and ZFC response of the fluctuation-dominated ($\eta = 0.2$) and anisotropy-dominated ($\eta = 4.0$) systems, in an applied field $h_a = 0.04$. In both cases, the magnetic response is characterized by a

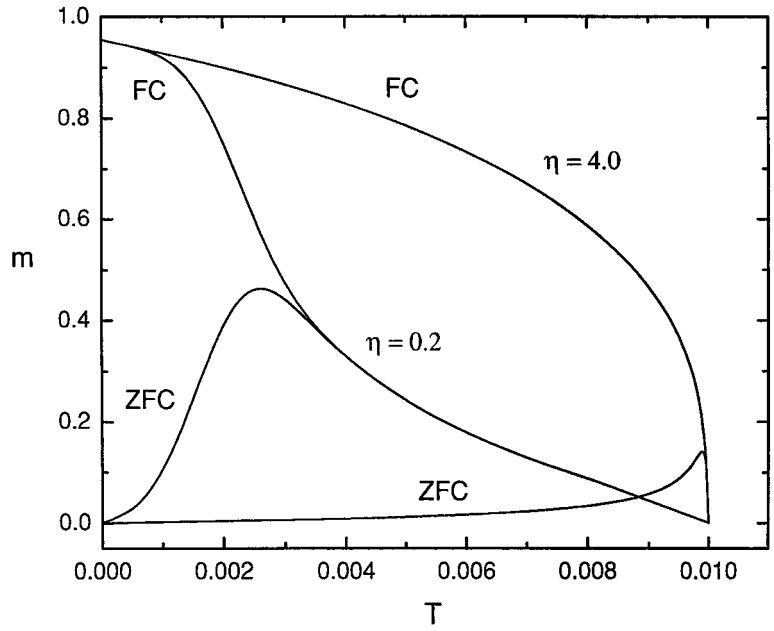

Figure 5. The temperature dependence of the FC and ZFC response functions in an applied field $h_a = 0.04$ for a fluctuation-dominated system with $\eta = 0.2$ and an anisotropy-dominated system with $\eta = 4.0$.

bifurcation temperature, below which the FC and ZFC moments follow different branches, with the FC moment always lying *above* the ZFC moment, and above which the two branches merge into a single superparamagnetic tail which extends up to T_C. The ZFC branch always exhibits a peak as a function of temperature. The physical origin of this peak is ultimately thermally activated overbarrier relaxation. The moment initially increases with temperature, as subsystems with interaction fields $-h_a \leqslant h_i \leqslant 0$ in figure 2 are activated from the $-\mu(T)$ state to the $+\mu(T)$ state through the thermal boundary h^*_{TS}, either by the motion of the boundary itself or by the collapse of the Preisach distribution. Eventually, however, the total system moment must decrease as the subsystem spontaneous moment $\mu(T)$ weakens and also as progressively more of the subsystems reach equilibrium and respond superparamagnetically as $\varphi_{sp} = \mu(T)\tanh[\mu(T)(h_a + h_i)/k_BT]$. However, in fluctuation-dominated systems, the *temperature dependence* of this structure is determined by sources *extrinsic* to the system, that is, by changes in the thermal fluctuation energy $W^*(T)$ with temperature, and hence by the *motion* of the thermal boundaries in figure 2. By contrast, in anisotropy-dominated systems, the characteristics of the peak are determined almost entirely by changes in the *intrinsic properties of the subsystems* $\mu(T)$ and $\bar{h}_c(T)$ and $\sigma_c(T)$ with temperature, and thus by the power law dependences in equation (3), although some fluctuation-assisted reduction of the barrier heights is unavoidably present. In order to illustrate this point, we show in figure 6 a comparison of the ZFC response of both systems in two applied fields $h_a = 0.04$ and $h_a = 0.4$, with the usual power law temperature dependences for the subsystem parameters $\Gamma_c = \Gamma'_c = \Gamma_i = \frac{1}{3}$ (solid curves), and with these intrinsic temperature dependences removed entirely, $\Gamma_c = \Gamma'_c = \Gamma_i = 0$ (dotted curves). Clearly, the effect on the fluctuation-dominated system is negligible, while, for the anisotropy-dominated system, 'freezing' the distribution essentially eliminates the peak.

The mean zero-temperature anisotropy barrier $\overline{W}_a(0) = \mu_0\bar{h}_{c0}$ plays an important role in defining the *location* of the peak in the ZFC response. This is illustrated in figure 7, which shows

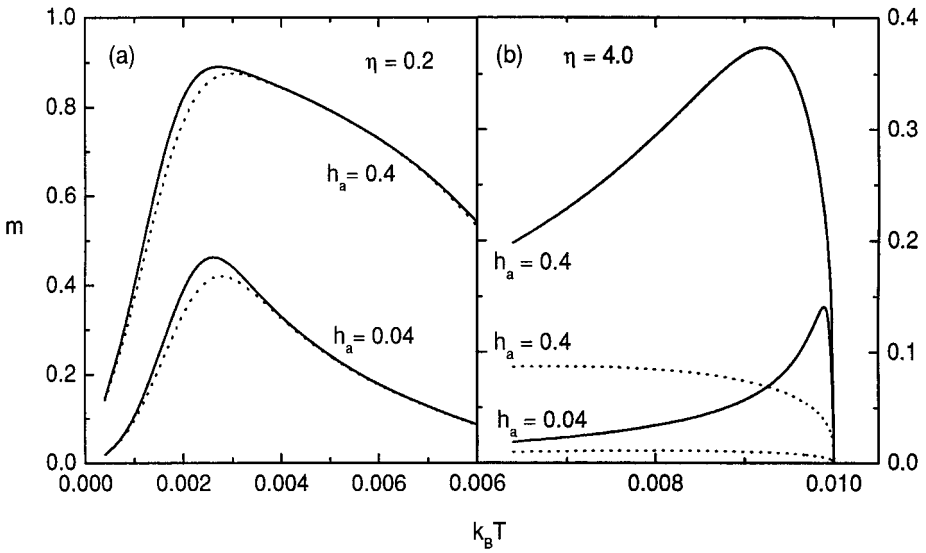

Figure 6. A comparison of the behaviour of the ZFC moment for the fluctuation-dominated and anisotropy-dominated systems in two applied fields $h_a = 0.04$ and $h_a = 0.4$, with the usual subsystem exponents $\Gamma_c = \Gamma'_c = \Gamma_i = 1/3$ (solid curves) and with the intrinsic temperature dependences removed entirely, $\Gamma_c = \Gamma'_c = \Gamma_i = 0$ (dotted curves).

the FC and ZFC response in both the fluctuation-dominated and anisotropy-dominated regimes, for various values of the spontaneous moment μ_0. For the fluctuation-dominated systems in figure 7(a), where the barrier distribution evolves very slowly with temperature, the temperature of the peak corresponds closely to the temperature at which $W^*(T)$ matches the mean zero-temperature anisotropy barrier $\overline{W}_a(0)$, that is $W^*(T_{peak}) = k_B T_{peak} \ln(t_{exp}/\tau_0) \cong \overline{W}_a(0)$, which yields an immediate estimate for the mean zero-temperature Barkhausen moment $\mu_0 \cong (k_B T_{peak}/\bar{h}_{c0}) \ln(t_{exp}/\tau_0)$. For the anisotropy-dominated systems in figure 7(b), the collapse of the free energy landscape and the spontaneous moment complicates this relationship considerably, and estimates of μ_0 depend on much more subtle structural features, such as the temperature dependence of the ZFC response *below* the peak.

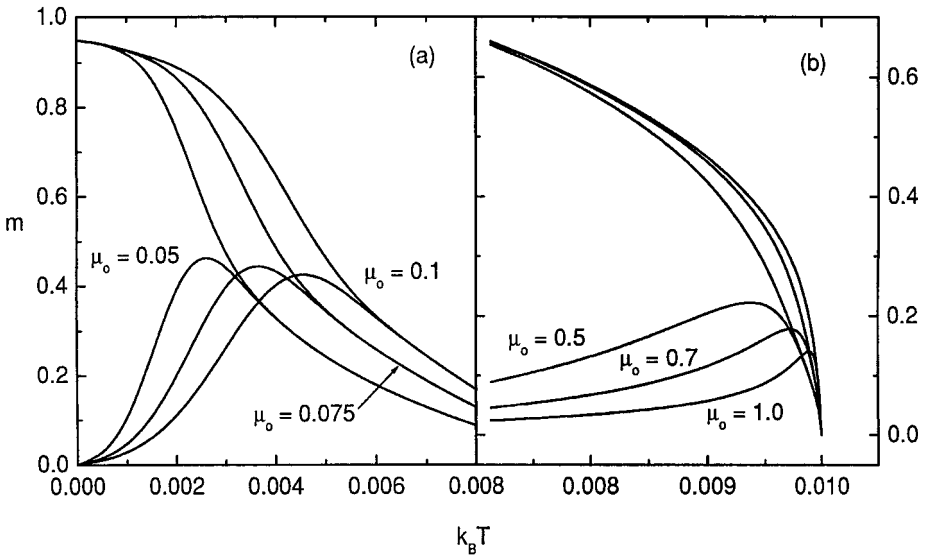

Figure 7. The dependence of the FC and ZFC response on the spontaneous subsystem moment μ_0 for (a) fluctuation-dominated systems and (b) anisotropy-dominated systems, in an applied field $h_a = 0.04$.

Interaction fields play a particularly important role in shaping the temperature dependence of the magnetic response, particularly the FC branch. Figure 8 shows the effect of varying the dispersion σ_{i0} of interaction fields for both fluctuation-dominated and anisotropy-dominated systems, in an applied field $h_a = 0.04$. When $\sigma_{i0} \ll h_a \ll \bar{h}_{c0}$, cooling from a high temperature blocks virtually all of the subsystems in figure 2 into their $+\mu(T)$ state, and the temperature dependence of the FC branch is determined either by the superparamagnetic response function $\tanh(a/T)$ if the system is fluctuation dominated (figure 8(a)), or by the critical temperature dependence of the spontaneous moment $\mu(T)$ if the system is anisotropy dominated (figure 8(b)). As σ_{i0} increases, the fraction of subsystems which are blocked into the $-\mu(T)$ state grows progressively larger, and the cancellation of the positive and negative moments causes the FC branch to deviate progressively further below the limiting curves for weak interactions ($\sigma_{i0} \ll h_a$). Figure 8 also shows that, by comparison with the FC response, interactions have a relatively minor influence on the characteristics of the ZFC branch, which tends to be dominated by anisotropy effects, as discussed earlier. Systematics like those predicted in figure 8(a) are familiar from a number of experimental studies of fine particle assemblies which manipulate the level of particle clustering [6, 7]. A detailed comparison of

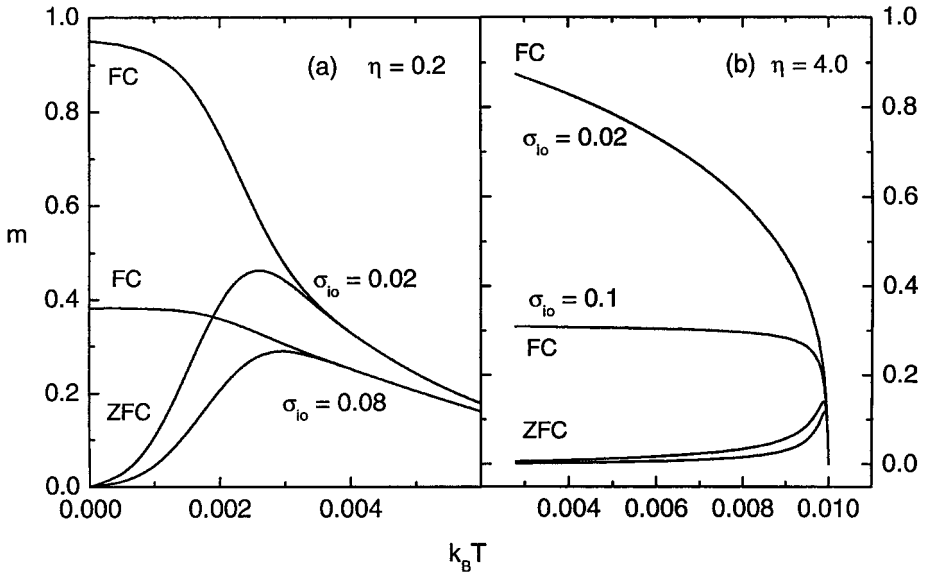

Figure 8. The dependence of the FC and ZFC response on the dispersion σ_{i0} of interaction fields for (a) a fluctuation-dominated system and (b) an anisotropy-dominated system. The applied field is $h_a = 0.04$.

these experimental and theoretical systematics has been presented in an earlier publication [8], using a version of the model which neglects the temperature dependence of the spontaneous moment and of the barrier distribution. Similarly, the systematic trends in figure 8(b) have recently been observed in several ferromagnetic perovskites [9], with $SrRuO_3$ representing the limit of weak interactions ($\sigma_{i0} \ll h_a$) and $Ni_{0.8}Zn_{0.2}Fe_2O_4$ representing the opposite limit of a strongly interacting system ($\sigma_{i0} \gg h_a$).

The *temperature dependence* of the interaction field distribution also has a profound effect on the shape of the FC and ZFC response functions, and figure 9 shows how the response functions of both fluctuation-dominated and anisotropy-dominated systems vary with the interaction field exponent Γ_i which controls the dispersion $\sigma_i(T) = \sigma_{i0}(1 - T/T_C)^{\Gamma_i}$. For values of $\Gamma_i < 1$, the *curvature* of $\sigma_i(T)$ is *negative* ($d^2\sigma_i/dT^2 < 0$), so the interaction fields vary relatively slowly with temperature, except in the immediate vicinity of T_C, where $|d\sigma_i/dT| \to \infty$, and the FC moment changes monotonically with temperature. However, for $\Gamma_i > 1$, the curvature $d^2\sigma_i/dT^2$ is *positive*, so the temperature dependence of the interaction fields is strong at low temperatures and the interaction fields become negligible well below T_C. Under these latter conditions the FC moment may exhibit a *peak* as a function of temperature if the collapse of the interaction field distribution, which increases the moment by increasing the number of subsystems in figure 2 with interaction fields $h_i \geqslant -h_a$ and hence with positive moments $+\mu(T)$, is sufficiently rapid to counteract either the superparamagnetic response $\tanh(a/T)$ from the shaded region in figure 2, or the critical collapse of the spontaneous moment $\mu(T)$. While, in principle, this effect is observable in both fluctuation-dominated and anisotropy-dominated systems, as shown in figure 9, rapid changes in the strength of the interaction fields *well below* T_C are difficult to justify on physical grounds for anisotropy-dominated systems, since in these systems it must ultimately originate from rapid changes in the spontaneous moment $\mu(T)$. However, in fluctuation-dominated systems, the crossover to superparamagnetism tends to occur well below T_C and provides a physically plausible source

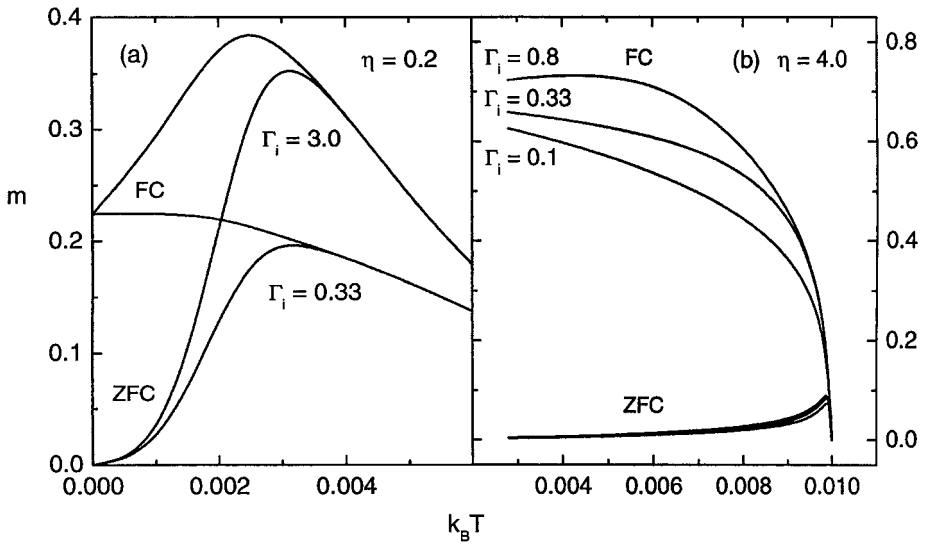

Figure 9. The dependence of the FC and ZFC response on the interaction field exponent Γ_i for (a) a fluctuation-dominated system with $\sigma_{i0} = 0.14$ in an applied field $h_a = 0.04$ and (b) an anisotropy-dominated system with $\sigma_{i0} = 0.02$ in an applied field $h_a = 0.02$.

for a rapid weakening of the interaction fields.

Figure 10 shows the temperature dependence of the major hysteresis loop in both fluctuation-dominated and anisotropy-dominated systems. For the fluctuation-dominated system ($\eta = 0.2$) the collapse of the hysteresis loop is driven almost exclusively by extrinsic thermal fluctuation effects, while for the anisotropy-dominated system ($\eta = 4.0$), the collapse is defined by the intrinsic temperature dependences in equation (3). The Preisach simulations also reveal an interesting structural anomaly in the major hysteresis loops at 'high' temperatures, which is particularly apparent in the hysteresis isotherms of the fluctuation-dominated system in figure 10(a). When the system is warmed close to the reversible superparamagnetic regime, the hysteresis loop develops a *constriction* in the vicinity of the origin. This type of distortion is referred to in the literature as 'wasp-waisting' [10] or 'pinching' [11]. Such distortions of the hysteresis loop from 'textbook' behaviour are frequently encountered in geological materials, which tend to be heterogeneous mixtures of various minerals, grain sizes and domain configurations. Similar distortions have also been observed in a number of weakly interacting frozen ferrofluids [11–14], where they have been attributed to resonant tunnelling [15]. Wasp-waisted loops have been modelled theoretically [10] by superposing magnetic responses from two or more subpopulations of particles, which are distinguished from each other either on the basis of vastly different coercive fields, or by superparamagnetic versus single-domain response. The Preisach model offers a uniquely integrated approach to hysteresis, in which competitions like these are treated within a *single unified* theoretical framework. As a consequence, the model offers a unique insight into the physical origins of loop asymmetries. For the systems investigated here, wasp-waisting originates entirely from *thermal relaxation*. In terms of the Preisach diagrams in figure 2, when the system recoils from positive saturation to the saturated remanence state, the switching boundary $\beta = h_a$ sweeps downward through the Preisach plane from $\beta = \infty$ to $\beta = 0$, forcing all particles with $\beta > 0$ into the $\varphi = -\mu$ state, and leaving a saturation remanence at $T = 0$ equal to the sum of all the particle moments within the fourth quadrant of the

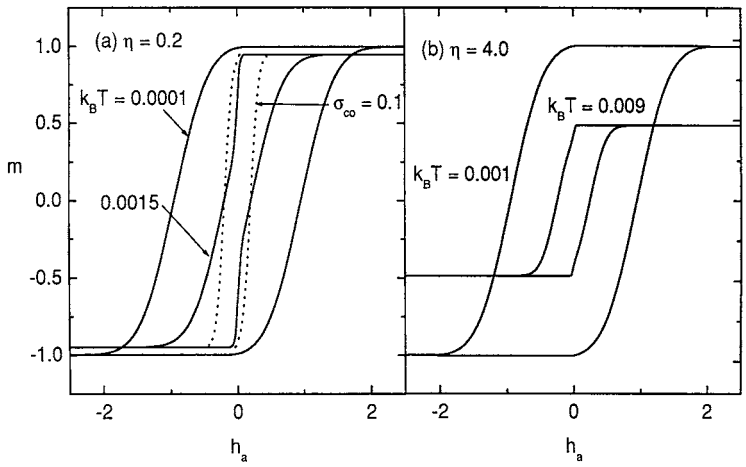

Figure 10. The temperature dependence of the major hysteresis loop for (a) a fluctuation-dominated and (b) an anisotropy-dominated system. The solid curves correspond to $\sigma_{c0} = 0.4$. The dotted curve in (a) shows the change in the $k_BT = 0.0015$ hysteresis isotherm when the coercive field dispersion is reduced to $\sigma_{c0} = 0.1$.

plane. This remanence differs only slightly from the saturation moment, since the Preisach distribution tends to be concentrated within the fourth quadrant. When $T \neq 0$, the two dashed thermal activation boundaries h^*_{TS} in figure 2 partition the fourth quadrant into a thermally relaxed, *demagnetized* component, and a thermally blocked, remanent component. When h^*_T is comparable to the mean coercive field $\bar{h}_c(T)$, thermal relaxation demagnetizes a significant portion of the fourth quadrant, and the moment drops precipitously when h_a approaches zero from above. The approach to negative saturation along the negative half branch of the major loop is more gradual, since the activation boundary $h^*_{TS} = h_c - |h_i + h_a|$ must now invert roughly *half* of the Preisach distribution, which requires negative fields $h_a \cong h^*_T - \bar{h}_c - \sigma_c - \sigma_i \cong -\sigma_c - \sigma_i$. The steepness of the major loop for $h_a < 0$ is thus directly dependent on the *dispersions* σ_c and σ_i of *coercive fields and interaction fields*. A broad distribution will tend to delay the approach to negative saturation and 're-open' the loop, producing the 'wasp-waisted' or 'pinched' appearance. The dotted curve in figure 10(a) illustrates the effect of varying the dispersion of coercive fields σ_{c0} on the hysteresis isotherm $k_BT = 0.0015$ for the fluctuation-dominated system, and clearly shows that when the distribution of coercive fields becomes sufficiently narrow, the 'wasp-waisting' becomes unobservable.

4. Comparisons with real systems

The model is able to replicate the response functions of specific systems, and thus offers a theoretical framework for establishing the properties of the Barkhausen spectrum and details of interaction effects in real materials. As specific illustrations, figures 11–13 show fits (solid curves) to representative FC/ZFC and hysteresis loop data (discrete points) for two thin films consisting of nanodimensional particles of Fe embedded in SiO_2 and in Al_2O_3, each with volume fractions $p \sim 0.3$, and a ferromagnetic substituted perovskite $La_{0.5}Sr_{0.5}CoO_3$, respectively. The best fit parameters for all three systems are listed in table 1. In order to describe the hysteresis loops, it was necessary to supplement the Preisach calculation by a purely reversible term which represents processes which are independent of field history, such

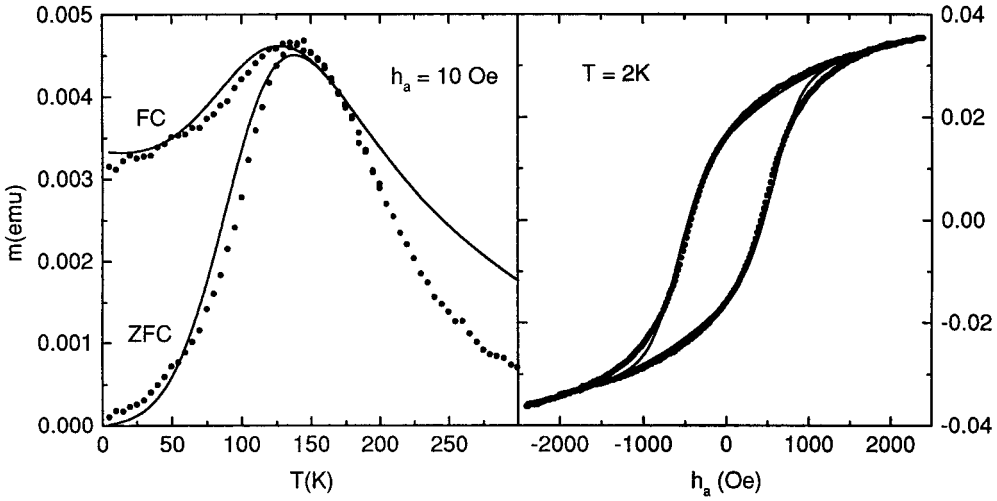

Figure 11. A comparison of Preisach simulations (solid curves) and experimental FC/ZFC and hysteresis loop data (discrete points) for a thin film of nanodimensional Fe particles embedded in SiO_2.

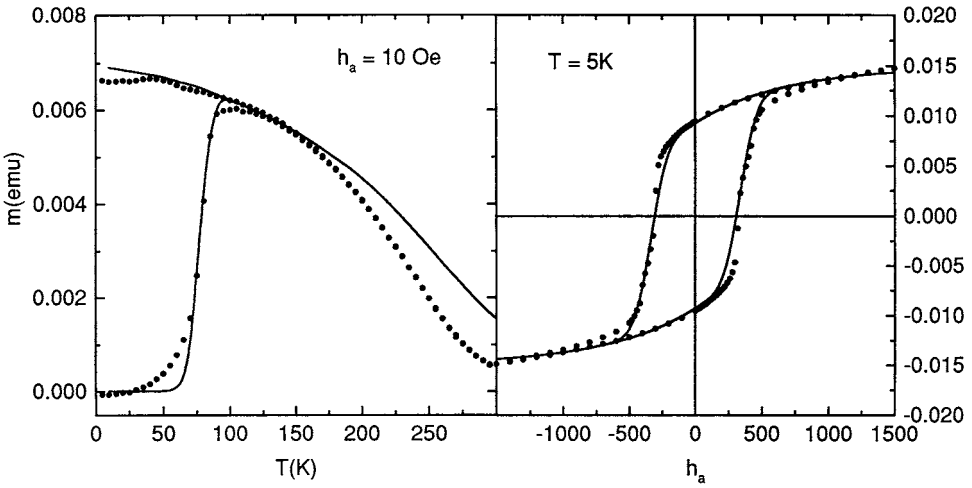

Figure 12. A comparison of Preisach simulations (solid curves) and experimental FC/ZFC and hysteresis loop data (discrete points) for a thin film of nanodimensional Fe particles embedded in Al_2O_3.

as elastic distortions of domain structure, or large populations of very small energy barriers which behave quasi-reversibly, or moment rotation due to a misalignment of the easy axis and the applied field [2]. Thus $m = m_{sat}[(1 - f)(\text{Preisach}) \pm f(1 - \exp(-\lambda|h_a|))]$.

A brief comment concerning the fitting procedure is in order here. In multi-parameter fits like these, which involve up to 13 parameters, an internally consistent, physically meaningful set of parameter values for a given system can be achieved only if the fits are performed to a *series* of hysteresis loops measured over a range of temperatures spanning the irreversible regime, as well as to a *series* of FC/ZFC response curves measured over a range of applied fields which extends at least up to the zero-temperature coercive field. The individual fits

Table 1. Best fit Preisach parameters.

System	T_C (K)	$\bar{h}_{c0}$ (Oe)	σ_{c0} (Oe)	σ_{i0} (Oe)	μ_0 (emu)	k (Oe emu^{-1})	Γ	Γ_c	Γ'_c	Γ_i	f	λ (Oe^{-1})	m_{sat} (emu)
Fe–SiO_2	500	600	240	60	5.0×10^{-16}	0	0.33	0.33	0.33	2.5	0.6	0.000 65	0.04
Fe–Al_2O_3	400	360	36	90	8.0×10^{-16}	8.4×10^3	0.33	0.33	0.33	0.33	0.38	0.0015	0.015
$La_{0.5}Sr_{0.5}CoO_3$	230	2000	0.8	200	5.0×10^{-16}	0	0.35	0.3	0.8	0.08	0.38	0.000 16	3.3

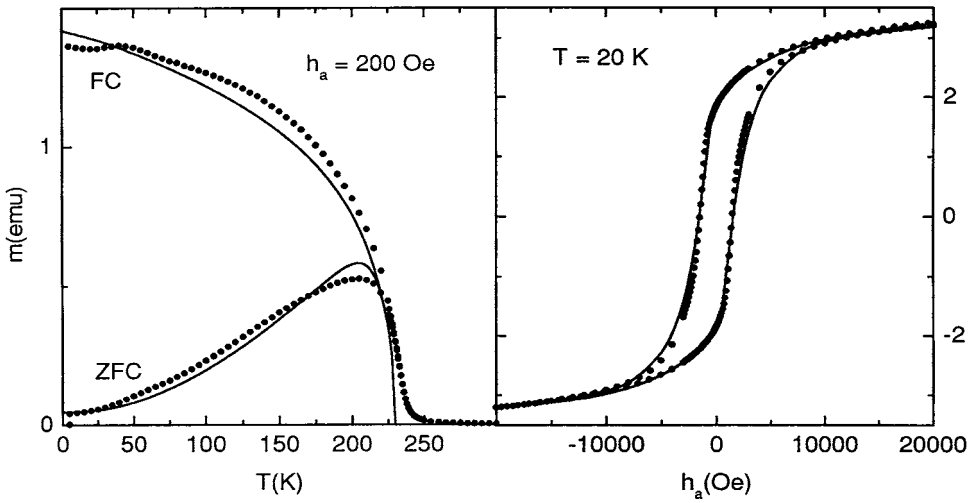

Figure 13. A comparison of Preisach simulations (solid curves) and experimental FC/ZFC and hysteresis loop data (discrete points) for a ferromagnetic perovskite $La_{0.5}Sr_{0.5}CoO_3$.

shown here are representative of such a sequence. Some of the parameters, such as the mean zero-temperature coercive field $\bar{h}_{c0}$, the saturation moment m_{sat}, the reversible parameters f and λ, and, in the case of ferromagnets, the critical temperature T_C, are defined more or less directly by the experimental data. While the remaining parameters are not decoupled, the numerical simulations indicate that the influence of each parameter tends to be limited *primarily* to certain specific features of the response. Thus, the curvature of the major loop defines σ_{c0} and Γ'_c, the FC branch defines σ_{i0}, k, Γ and Γ_i, while the major loop coercive field and the ZFC branch together define μ_0 and Γ_c.

The fits to the Fe–SiO_2 thin film in figure 11 show that this system is characterized by Barkhausen elements with a mean zero-temperature spontaneous moment $\mu_0 = 5.0 \times 10^{-16}$ emu $\approx 50\,000\ \mu_B$, and a mean zero-temperature coercive field $\bar{h}_{c0} = 600$ Oe with a dispersion $\sigma_{c0} = 240$ Oe, corresponding to a mean zero-temperature anisotropy barrier $\overline{W}_a(0) = \mu_0 \bar{h}_{c0} = 3.0 \times 10^{-13}$ erg. Since μ_0 is several orders of magnitude larger than the moment expected for a single Fe grain of diameter $d \cong 3$ nm, we conclude that the Barkhausen entity probably consists of a strongly coupled *cluster* of Fe particles, which responds as a cohesive unit. The Barkhausen elements experience local random interaction fields with a dispersion $\sigma_{i0} = 60$ Oe. This system is unusual in the sense that the FC response also exhibits a well defined peak, which coincides with the peak in the ZFC branch. The fits show that this behaviour is a direct consequence of the *temperature dependence of the interaction field distribution*, specifically $\sigma_i(T)$. While a power law of the form $\sigma_i(T) = \sigma_{i0}(1 - T/T_C)^{\Gamma_i}$ with $\Gamma_i \cong 2.0$ can provide an approximate representation of the data, the fits in figure 11 employed a stretched exponential $\sigma_i(T) = \sigma_{i0} \exp[-(T/T_{BL})^{\Gamma_i}]$ with $\sigma_{i0} = 60$ Oe, $T_{BL} = 130$ K and $\Gamma_i = 2.5$. In either case, the interaction field distribution collapses rapidly with increasing temperature in the vicinity of the peak, leading to an enhancement of the FC moment, as predicted earlier by the numerical simulations in figure 9. The fits also yield a value of $\eta = \overline{W}_a(0)/W_C = 0.18$, which clearly places this system within the fluctuation-dominated category. This is consistent with the relative insensitivity of the fits to any of distribution exponents Γ, Γ_c, Γ'_c and Γ_i, and hence to the details of the collapse of the free energy landscape.

The analysis of the Fe in Al_2O_3 data in figure 12 shows a similar tendency for the Fe particles to cluster into large Barkhausen units with moment $\mu_0 = 8 \times 10^{-16}$ emu, and yields similar anisotropy barriers $\overline{W}_a(0) = 2.9 \times 10^{-13}$ erg and a similar ratio of $\eta = \overline{W}_a(0)/W_C = 0.2$, indicative of a fluctuation-dominated system. However, the characteristics of the *interaction* field distribution differ markedly in the two systems. The interaction field energy $\mu_0\sigma_{i0}$ is more than a factor of two larger in the Fe–Al_2O_3 system and there is no evidence for a rapid collapse of the interaction fields with temperature, as observed in the Fe–SiO_2 system. Furthermore, the Fe–Al_2O_3 system is characterized by a long-ranged *ferromagnetic* coupling between the Barkhausen units with a mean-field coupling constant $k = +8.4 \times 10^3$ Oe emu^{-1}, so the mean interaction field $\bar{h}_i = km$ experienced by a Barkhausen element varies from $\bar{h}_i = 0$ to $\bar{h}_i = 126$ Oe between the initial demagnetized state and saturation.

In contrast with that of the thin films, the behaviour of the perovskite system in figure 13 clearly reflects the influence of the critical temperature T_C. The fits in figure 13 were generated using a log-normal distribution of coercive fields $(2\pi h_c^2\sigma_c^2)^{-1/2}\exp[-(\log(h_c/\bar{h}_c))^2/2\sigma_c^2]$, and yielded a Barkhausen moment $\mu_0 = 5.0 \times 10^{-16}$ emu, and a median coercive field $\bar{h}_{c0} = 2000$ Oe, corresponding to a median anisotropy barrier $\overline{W}_a(0) = 1.0 \times 10^{-12}$ erg. This system has a granular microstructure, and the effective Barkhausen moment μ_0 is many orders of magnitude smaller than the saturation moment of a typical grain of size $d \cong 40$ μm, which suggests that moment reversal in this system probably proceeds through local unpinning of domain walls within the grains. For this system, $\eta = \overline{W}_a(0)/W_C = 1.7$, which indicates that intrinsic effects play a dominant role in shaping the response, although thermal fluctuations clearly are not negligible. In fact, our fits show that the gradual slope of the ZFC moment below the peak is a direct consequence of the motion of the thermal relaxation boundaries h^*_{TS} in figure 2, which is strongly influenced by the size of μ_0. The analysis also reinforces the dichotomy of the FC and ZFC response, in the sense that the amplitude and shape of the FC branch are determined primarily by σ_{i0} and the exponents Γ and Γ_i, while the ZFC branch is dominated by anisotropy effects through σ_{c0}, $\bar{h}_{c0}$, Γ_c and Γ'_c.

5. Summary

The Preisach model of hysteresis has been used as the basis for developing a general theoretical description of irreversibility in magnetically ordered systems, which includes the effects of the critical ordering temperature T_C. The free energy landscape is decomposed into an ensemble of two-level metastable subsystems, each characterized by two energy barriers which are defined by the local anisotropy and interaction fields. The free energy landscape has an explicit temperature dependence which originates from the critical growth of the spontaneous moment below T_C, and thermal overbarrier fluctuations are responsible for relaxing the system towards equilibrium. These physical elements are basic to all systems which exhibit hysteresis. The Preisach model unifies these essential elements within a single comprehensive theoretical framework, which provides a precise and uniquely visual representation of fundamental processes such as thermal blocking, and which includes an elegant mathematical algorithm for computing the magnetic response of the system under a variety of experimental protocols. The model characterizes all magnetic systems by a set of *fundamental parameters* which include the critical magnetic ordering temperature T_C, the spontaneous moment μ_0 and the mean coercive field $\bar{h}_{c0}$ of the component subsystems at $T = 0$, the dispersion of subsystem coercive fields σ_{c0} and the dispersion of subsystem interaction fields σ_{i0} at $T = 0$, and the exponents Γ, Γ_c, Γ'_c and Γ_i which define the temperature dependence of the spontaneous moment and the distributions of coercive and interaction fields. In order to illustrate the broad spectrum of

magnetic behaviour encompassed by the formalism, we have focused on two limiting classes of magnetic systems. This classification is based on a comparison of two characteristic energies, the mean zero-temperature anisotropy barrier of the subsystems $\overline{W}_a(0) \equiv \mu_0 \bar{h}_{c0}$ and the 'critical' thermal fluctuation barrier $W_C \equiv k_B T_C \ln(t_{exp}/\tau_0)$, which, according to the model, play a pivotal role in determining the principal features of the magnetic response. The systems studied here represent the two extreme situations where $\overline{W}_a(0) \gg W_C$ and $\overline{W}_a(0) \ll W_C$.

Perhaps the most striking feature of the model is the richness and scope of its predictive capabilities. The model is able to replicate a broad spectrum of behaviour observed experimentally in the field and temperature dependence of magnetic response functions like the FC and ZFC moment and the major hysteresis loop, in a wide variety of magnetic materials. The model is able to reproduce very specific experimental anomalies and trends, and to quantify the interpretation of these systematics by linking them to specific physical parameters and characteristic energies. One of the unique features of Preisach-based models like this one, is the explicit treatment of *interaction effects*. These interactions are an *intrinsic* component of the formalism, which arise from the *asymmetry* of the double well potentials which make up the free energy landscape of the material. Interparticle interactions are always present to some extent in all materials, and the simulations show that many of the experimental systematics ultimately originate from changes in the *dispersion* σ_{i0} of *local random static interaction fields*, presumably due to modifications in the local environment of the particles. Future work will focus on incorporating a distribution $f(\mu)$ of particle moments μ in order to simulate the distribution of particle sizes observed in real systems. This is a nontrivial generalization, since each element $\mu \rightarrow \mu + \mathrm{d}\mu$ of the distribution is activated by a different viscosity field h_T^*, and requires its own Preisach diagram.

Acknowledgment

The authors would like to acknowledge Professor Shihui Ge, Department of Physics and Materials Science, Lanzhou University, People's Republic of China, for supplying the particulate thin film materials analysed here.

References

[1] Preisach F 1935 *Z. Phys.* **94** 277
[2] Bertotti G 1998 *Hysteresis in Magnetism* (New York: Academic)
[3] Néel M L 1950 *J. Physique Radium* **11** 49
[4] Souletie J 1983 *J. Physique* **44** 1095
[5] Della Torre E 1966 *IEEE Trans. Audio Electroacoust.* **14** 86
[6] Dormann J-L, Fiorani D and Tronc E 1987 *Adv. Chem. Phys.* **98** 283
[7] Prené P, Tronc E, Jolivet J-P, Livage J, Cherkaoui R. Noguès M, Dormann J-L and Fiorani D 1993 *IEEE Trans. Magn.* **29** 2658
[8] Song T and Roshko R M 2000 *IEEE Trans. Magn.* **36** 223
[9] Joy P A, Anil Kumar P S and Date S K 1998 *J. Phys.: Condens. Matter* **10** 11 049
[10] Tauxe L, Mullender T A T and Pick T 1996 *J. Geophys. Res.* **101** 571
[11] Friedman J R, Voskoboynik U and Sarachik M P 1997 *Phys. Rev.* B **56** 10 793
[12] Luo W, Nagel S R, Rosenbaum T F and Rosensweig R E 1991 *Phys. Rev. Lett.* **67** 2721
[13] Tejada J, Zhang X X, del Barco E, Hernandez J M and Chudnovsky E M 1997 *Phys. Rev. Lett.* **79** 1754
[14] Hanson M, Johansson C and Morup S 1995 *J. Phys.: Condens. Matter* **7** 9263
[15] Friedman J R, Sarachik M P, Tejada J and Ziolo R 1996 *Phys. Rev. Lett.* **56** 3830